07

Modification of a standard Al-BSF solar cell line into PERC using PECVD

© I.A. Klinovitskaya,[1] S.V. Plotnikov,[1] P.M.L. Lay[2]

[1] D. Serikbayev East Kazakhstan technical university, Ust-Kamenogorsk, Kazakhstan
[2] ECM Technologies, 46 rue Jean Vaujany — Technisud,
F-38029 Grenoble, France
e-mail: iklinovitskaya@inbox.ru

Received July 29, 2021
Revised January 20, 2022
Accepted January 20, 2022

This study is devoted to comprehensive study of the physical and electrical properties of solar cells manufactured on the basis of the Kazakhstan multicrystalline silicon of solar grade (SoG-Si). The study applied: 4-point resistance measurement method, a method of microwave detected photoconductive decay (?-PCD), a method of Light Beam Induced Current (LBIC), methods for spectrometric analysis of reflection, transmission and photoluminescence coefficients, scanning electron microscopy, and methods for analyzing current-voltage characteristics. The batches of Al-BSF and PERC photovoltaic converters based on Kazakhstani silicon were manufactured and analyzed. To improve efficiency, the study proposes a modification of a standard Al-BSF production line to a PERC line using PECVD.

Keywords: solar cell, silicon, efficiency, Al-BSF, PERC, solar cell production, PECVD.

DOI: 10.21883/TP.2022.04.53606.224-21

Introduction

Presumably, the photovoltaic energy conversion will be of paramount importance on the power market in the future. According to projections of the United Nations, the world population will grow from 7.7 billion to 9.2 billion people in 2040; therefore, the global energy demand will continue to increase [1]. Specifically, the global energy consumption will increase by 28%. Solar energy is the most important and intense source of energy available to mankind.

Photovoltaic converters (PVCs) based on crystalline silicon (*c*-Si) are the most widespread type of PVCs: they occupy about 90% of the entire market of photovoltaic systems. This technology provides the highest efficiency of energy conversion of all commercially available PVCs and is expected to remain dominant on the market of photovoltaic systems in the future [2].

As part of the transition to „green“ economy, Kazakhstan has initiated the project aimed at fabrication of photovoltaic modules based on the Sarykol quartz deposit in 2010 [3,4]. The raw material (silicon) is produced in a carbothermic process at the KazSilicon metallurgical complex in Ushtobe. The fabrication of PVCs and the assembly of modules are performed at the Kazakhstan Solar Silicon and Astana Solar plants in Oskemen and Nur-Sultan, respectively.

The present study is focused on the fabrication of PVCs. Its aim is to examine the properties and possible approaches to modification of the fabrication line for the purpose of production of highly efficient PVCs with an advanced architecture. The study of properties provides an opportunity to identify the factors reducing the PVC efficiency and the ways to increase it.

In recent decades, the Al-BSF technology accounted for 90% of the global PVC production. This technology is regarded as a standard and provides stable efficiency values and a reliable fabrication process [5].

The PERC PVC production technology is an update of the standard Al-BSF technology [6]. Its primary advantages over Al-BSF are the recombination suppression and the enhancement of reflectivity due to passivation of the rear surface of a converter. Owing to this passivation, light reaching the rear surface without generating free carriers is reflected back into a PVC and has an opportunity to generate more free electrons and electrical current [7,8].

The market share of the PERC design increases rapidly in the photovoltaic industry. The primary reason behind the switch to PERC is the efficiency enhancement (relative to Al-BSF). According to research data [2], the average efficiency of Al-BSF PVCs is 18%, while *c*-Si-based PERC PVCs provide an efficiency within the range of 21−24%. It should also be noted that PERC is compatible with the available equipment for PVC fabrication, making it rather easy to switch to this new technology. According to [2], the share of PERC PVCs on the global market in the photovoltaic industry was slightly above 30% in 2019 and should reach 50% in the 2020s. The forecasts of production of various types of PVCs are presented in Fig. 1.

Batches of Al-BSF and PERC PVCs were fabricated to examine the possibility of switching to the new technology. Silicon wafers (SWs) produced from polycrystalline solar-grade silicon (SoG Si) from Kazakhstan were chosen as the samples for study.

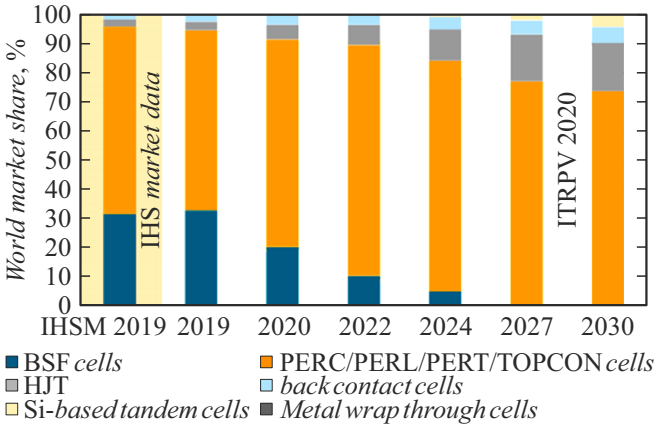

Figure 1. Shares of different technologies on the global market and development prospects [2].

1. Standard Al-BSF structure and fabrication methods

The production process of standard Al-BSF PVCs involves the following key stages [9]:

— texturization;

— phosphorus diffusion, formation of a $p-n$ junction;

— removal of phosphosilicate glass (PSG) and etching of the parasitic emitter;

— deposition of an antireflective coating by plasma-enhanced chemical vapor deposition (PECVD);

— fabrication of current-collecting bus lines and a contact grid (metallization) by screen printing;

— drying of the rear aluminum surface field and firing of contacts;

— measurement of the current–voltage curve (CVC) of finished PVCs.

Figure 2 shows the schematic diagram of the structure of a standard Al-BSF PVC.

SWs with a thickness of $180-200\,\mu$m, a resistivity of $\sim 2\,\Omega\cdot$cm, and a size of 156×156 mm were used to fabricate Al-BSF PVC samples. All wafers were subjected to acidic anisotropic texturization that involved the following stages: texturization in a solution of hydrofluoric acid (HF) with a concentration of 50% and nitric acid (HNO_3) with a concentration of 65% at a temperature of 10°C for 152 s; etching of the porous layer in an alkaline KOH solution with a concentration of 45% at a temperature of 20°C for 22 s; reduction and etching of metals in a solution of HF with a concentration of 50% and hydrochloric acid HCl with a concentration of 37% at a temperature of 22°C for 50 s. Two-step rinsing in deionized water was carried out after each stage. This SW surface texturization was performed in order to reduce significantly the reflection coefficient and the rate of surface recombination. The etching of metals in a solution of hydrofluoric and hydrochloric acids was performed in order to clean the surface of contaminants before the start of the next stage: phosphorus diffusion. The presence of a considerable amount of metal impurities and alkaline residues may translate into a large number of defects in a $p-n$ junction. The image of the SW surface before and after texturization obtained using a JSM-6390LV (Jeol, Japan) scanning electron microscope (SEM) is shown in Fig. 3.

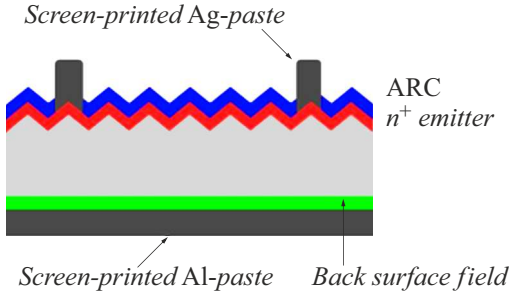

Figure 2. Schematic diagram of the structure of a standard Al-BSF PVC.

Regardless of the orientation of crystallites, dimples formed after texturization on both sides of SWs. The emergence of this surface structure in the form of dimples is attributable to the fact that polycrystalline silicon wafers do not have a common crystallographic orientation, while texturization was performed in an isotropic acidic solution.

At the next stage, an emitter ($p-n$ junction) was formed by phosphorus diffusion. Doping was performed under a pressure slightly below the atmospheric one at a temperature of 830–860°C. A Semco Engineering (Lydop) diffusion furnace was used to form an emitter in the course of the experiment. Phosphorus oxychloride ($POCl_3$) was fed into the furnace together with nitrogen and served as a source of phosphorus. The following decomposition reaction proceeds in the furnace in the presence of oxygen:

$$2POCl_3 + O_2 = 2P + 2O_2 + 3Cl_2. \quad (1)$$

It is followed by reactions

$$4P + 5O_2 = 2P_2O_5, \quad (2)$$

$$2P_2O_5 + 5Si = 5SiO_2 + 4P. \quad (3)$$

In general, the diffusion process may be divided into three stages [4]:

— formation of PSG on the wafer surface;

— phosphorus diffusion from PSG to the near-surface layer;

— phosphorus diffusion from the near-surface layer into the bulk of a sample.

The emitter was formed at a depth of $0.3-0.5\,\mu$m, the sheet resistance was $65\pm 5\,\Omega$/sq, and the average lifetime of minority charge carriers was $> 10\,\mu$s.

As is known [10], PSG and an n-layer form in the process of diffusion not only on the front surface of a wafer, but also on its rear surface and at its sides. This leads to electrical closure of front and rear current-collecting contacts. Therefore, silicon wafers were immersed in a

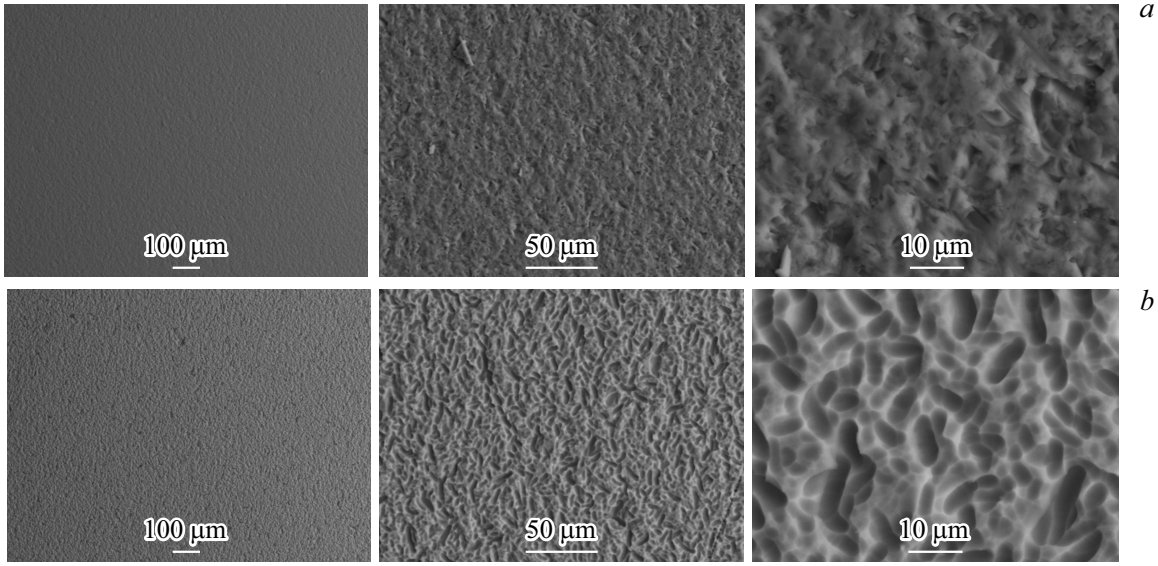

Figure 3. SEM image of the SW surface under different magnifications before (*a*) and after (*b*) texturization.

solution of hydrofluoric and nitric acids (HF/HNO_3) to remove PSG and etch away the parasitic emitter. The front surface was not exposed to the solution, and the rear *n*-layer was thus etched. Following etching, the wafers were treated with a KOH solution that was sprayed onto the front surface and wetted the rear surface. The layer of porous silicon was removed at this stage.

At the next stage, an antireflective coating (ARC) was deposited by PECVD onto the wafer surface. Silicon nitride (SiN_y) has become the most reliable passivation material for the front surface of PVCs, since it has excellent antireflective properties and provides polarizing passivation coupled with moderate suppression of surface states. The passivation of the front PVC surface with a SiN_y film deposited by PECVD provided an opportunity to achieve a record-low effective surface recombination rate [11]. This procedure is conducted in the presence of silane SiH_4 and ammonia NH_3 by producing a radio-frequency electrical field between opposite electrodes, thus initiating a gas discharge. Reactions characterized by the following equations then proceed within the reactor:

$$2SiH_4 + N_2 = 2SiNH + 3H_2, \quad (4)$$

$$SiH_4 + NH_3 = SiNH + 3H_2. \quad (5)$$

Simultaneously with the deposition of an ARC, passivation and hydrogenation of the bulk wafer material was performed by PECVD to enhance the efficiency. An extremely thin silicon nitride film, which has the needed properties, was „grown" on the front SW surface as a result. Its refraction index was $n = 2-2.15$ at a film thickness of about 70 nm.

In order to minimize the obscured area of the finished PVC surface, the screen printing method, which allows one to form relatively narrow contacts (the standard contact width is around $75-100\,\mu$m), was used to deposit bus lines and the contact grid. This method consists in pressing a conducting paste through special screens with a specific pattern. A silver-containing conducting paste with a sheet resistance below $2\,m\Omega/sq$ and a viscosity of $16-23\,Pa \cdot s$ was used for bus lines and the contact grid on the front PVC surface, and current-collecting bus lines on the rear surface were formed from a silver paste with a resistance of $5\,m\Omega/sq$ and a viscosity of $89\,Pa \cdot sa$. An aluminum paste with a resistance of $0.05\,\Omega/sq$ and a viscosity of $50-70\,Pa \cdot s$ was used to deposit the BSF.

Contact grids and bus lines were dried at a temperature of $200-250^\circ C$ after each step of paste deposition to evaporate the solvent. The firing of contacts was performed in a Despatch CDF Series (United States) belt IR furnace. Following preliminary heating, particles of a metal powder were welded together at a temperature of $500-600^\circ C$. The temperature was then raised to $710^\circ C$ to form the rear contact, and the front contact was formed last at the maximum temperature ($860^\circ C$).

2. PERC structure and fabrication methods

The PERC technology gradually becomes the most cost-effective choice for mass production of PVCs and provides efficiencies of *c*-Si-based PVCs in excess of 20% [12].

It should be noted that PVCs utilizing the PERC technology (PERC PVCs) are a natural evolution of Al-BSF PVCs. The schematic diagram of the PERC PVC structure is shown in Fig. 4.

Electrical and optical losses, which are typical of Al-BSF PVCs and reduce the efficiency of a standard PVC, may be excluded by depositing an additional dielectric passivation layer (DPL) onto the rear PVC surface. In the

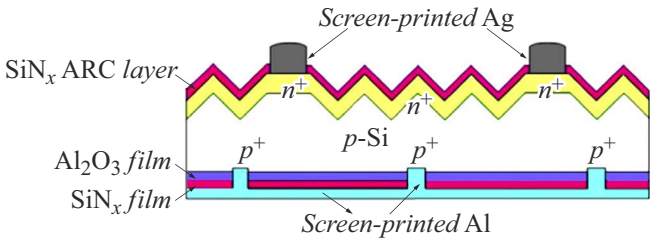

Figure 4. Schematic diagram of the PERC PVC structure.

present study, plasma-enhanced chemical vapor deposition was used to form Al_2O_3 and SiN_y films. This method consists in decomposing the reaction gases into radicals with gas-discharge plasma and depositing these radicals onto the surface of a silicon wafer.

Silicon wafers with a thickness of $180-200\,\mu$m, a resistivity of $\sim 1-2\,\Omega\cdot$cm, and a size of 156×156 mm were used to fabricate PERC PVC samples. The following sequence of process operations was chosen:

— texturization;

— phosphorus diffusion, formation of a $p-n$ junction;

— PSG removal, etching of the parasitic emitter, and polishing of the rear surface;

— deposition of the $AlO_x/SiO_xN_y/SiN_1/SiN_2$ coating onto the rear wafer surface by PECVD;

— deposition of the SiO_x/SiN_x double antireflective coating (D-ARC) onto the front wafer surface by PECVD;

— laser ablation (formation of the rear contact pattern);

— metallization by screen printing;

— firing of contacts by rapid thermal processing;

— measurement of CVCs of finished PVCs.

As was already noted, the fabrication of PERC PVCs involves the deposition of a passivation layer onto the rear PVC surface. This layer is then „opened“ using a laser to form the rear contact. These additional stages are crucial and the most important ones for switching from Al-BSF to PERC (Fig. 5). In addition, the stage of removal of the parasitic emitter and phosphosilicate glass needs to be optimized to polish (etch) the rear surface. Thus, one of the textured surfaces is removed by etching the pyramidal structure from the rear.

The emitter was formed at a depth of $0.4\,\mu$m by phosphorus diffusion (the method used to form the $p-n$ junction in Al-BSF PVCs). The sheet resistance was $90\pm 2\,\Omega$/sq, and the average lifetime of minority charge carriers was in excess of $10\,\mu$s. PSG removal, etching of the parasitic emitter, and polishing of the rear surface were performed using the wet chemical method with a $HNO_3-HF-H_2SO_4$ solution. The polishing time was on the order of 150 s, and the etched layer thickness was $1\,\mu$m. A polished rear surface enhances the SW light absorbance and ensures efficient surface passivation at subsequent stages.

A Twin PECVD for PERC Technology setup was used to deposit the rear passivation layer (Fig. 6). The general principle of PECVD and the radio-frequency power, which is used for precursor dissociation under low pressure and initiates the film deposition onto the wafer surface in the reactor, remained the same. A gas mixture of TMA (trimethylaluminium) and N_2O was used to deposit the AlO_x layer, and technological gases SiH_4 and NH_3 were used for $SiO_xN_y/SiN_1/SiN_2$ layers. It should be noted that the entire DPL was deposited in a single process step.

Aluminum oxide (AlO_x) with a high level of passivation is the passivation material of choice for the rear PVC surface. This oxide differs radically in its properties from the other dielectric materials commonly used for passivation. It features a high density of fixed negative charge (10^{13} cm^{-1}), while the other materials normally have a positive charge [14]. This high density of fixed negative charge is localized at the AlO_x/Si interface and ensures high polarizing passivation due to screening of electrons from the interface. The mentioned oxide also has fine chemical passivation properties: it acts as a hydrogen reservoir and supplies hydrogen for the saturation of dangling bonds on the wafer surface in the course of thermal processing. As for optical properties, AlO_x films with a bandgap of 6.4 eV are transparent in the part of the solar spectrum that is used in photovoltaics [15]. Their only drawback is a relatively low refraction index (1.65), which makes aluminum oxide less suitable for application as a single-layer antireflective film at the emitter side; however, the dielectric material serves as a fine back reflector.

The authors of [16] have revealed the dependence of effective lifetime τ_{eff} on the AlO_x layer thickness and determined the optimum thickness value (10–15 nm). The Twin PECVD setup allows one to adjust the layer thickness by increasing or decreasing the deposition time. The following layer thicknesses were chosen in the present study: AlO_x — 10 nm, SiO_xN_y — 30 nm, SiN_1 — 50 nm, SiN_2 — 100 nm. The deposition time was 45 min, and the temperature was $200-450^\circ$C.

In commercial production of PERC PVCs, the most important function of the SiN_y layer is maximizing the protection of AlO_x from aluminum paste applied by screen printing [17]. in addition, the process of deposition of the SiN_y film by PECVD contributes to activation of the AlO_x layer. The SiN_y film provides an opportunity to stabilize the AlO_x film annealing and ensures hydrogen passivation of the Si/AlO_x interface and the primary silicon layer. This has a positive effect on the open-circuit voltage and, to a certain extent, on the current production in a finished PVC.

Laser technology provides the easiest way to „open“ the rear passivation layer. A considerable number of laser solutions offered by such companies as InnoLas Solutions, Rofin, 3D-Micromac, Schmid, and Manz are currently available on the photovoltaic market. In the present study, the DPL was „opened“ by laser ablation.

The contact grid and bus lines were formed by screen printing (just as in the first batch of Al-BSF PVCs). However, specialized metallization pastes are required for PERC. The choice of a paste for the rear BSF surface is crucial for the process of metallization. The chosen paste

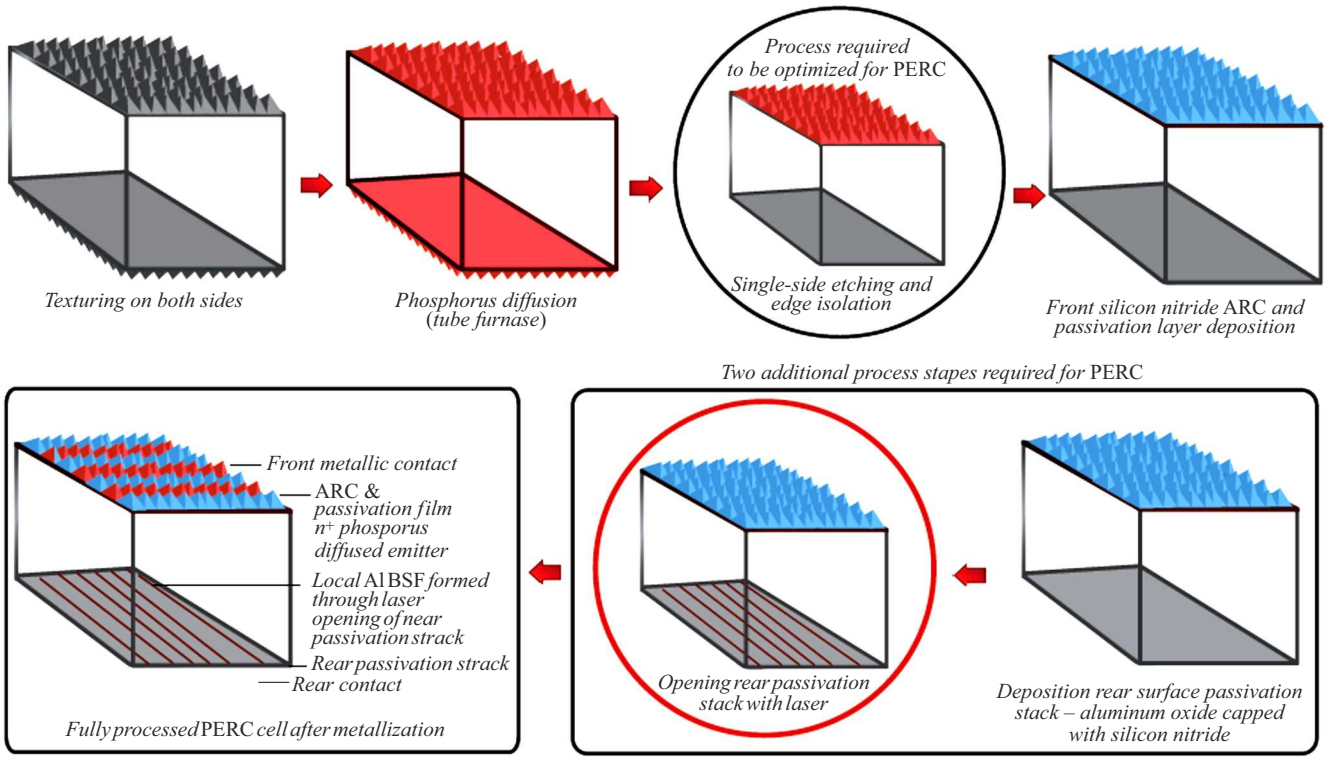

Figure 5. Diagram of the PERC PVC production process in comparison with the standard Al-BSF PVC production process [13].

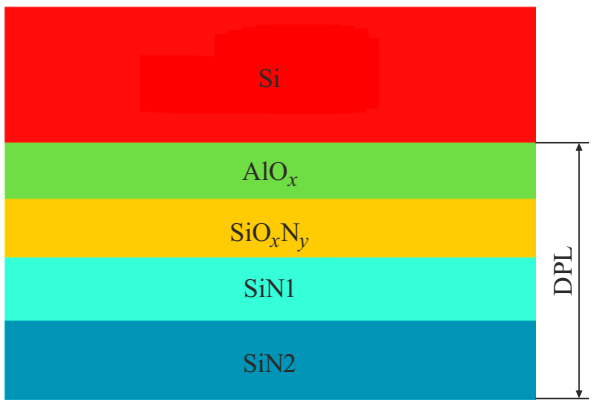

Figure 6. Diagram of the rear passivation layer.

should not react with the DPL, but, at the same time, should come into contact with regions „opened“ with a laser to form the local BSF. A chemically inert silver-containing paste for rear bus lines is also needed. This paste has two main features: it should not penetrate through the DPL and should have fine adhesion and solderability.

A pulsed tester with a xenon lamp was used in the present study to measure the electrical parameters (short-circuit current I_{sc}, open-circuit voltage U_{oc}, filling factor FF, maximum power P_{mpp}, efficiency, and shunt resistance R_{sh}). Calibrated flash lamps of the solar simulator irradiate a PVC, while an electronic load conditioner shifts the cell from the conditions of the maximum obtained current strength (short-circuit current) to the conditions of the maximum obtained voltage (open-circuit voltage). The Berger simulator computer accumulates data and calculates the PVC parameters. The provided software allows one to control the process of measurement of electrical PVC characteristics.

3. Examination and analysis of the properties of Al-BSF PVCs and PERC PVCs

The properties and parameters of SWs and PVCs were examined at Institut National de l'nnergie Solaire (INES) in France. At the first stage, the resistivity of SWs (an electrophysical parameter of the used semiconductor material) was measured. It should be noted that the studied SWs were used to fabricate batches of Al-BSF PVCs and PERC PVCs. The four-point probe measurement method, which does not require the formation of an Ohmic contact to the studied sample, is the most convenient in this case. It allows one to preserve the material and its properties in the process of measurement. Therefore, a CMT SR2000N four-point probe resistance measurement system was used to examine the resistivity. The measurement results are presented in Fig. 7.

Electrically active and inactive impurities exert a strong influence on the electrophysical characteristics of silicon and

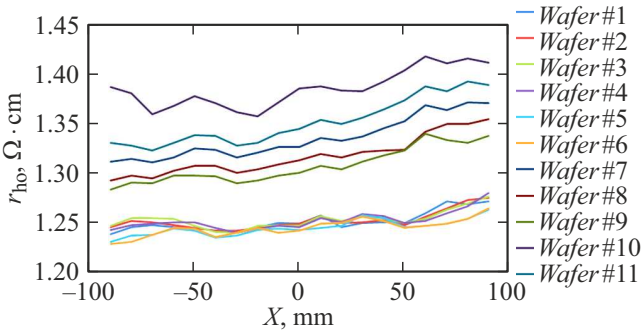

Figure 7. Resistivity of SWs prior to processing.

PVC parameters. They alter the lifetime and absorption coefficients, raise the rates of surface and bulk recombination, and alter the rate of diffusion of elements in the process of doping. The presence of impurities also has an effect on the resistivity of silicon and regions of a finished PVC. Figure 7 demonstrates that the resistivity of the studied SWs falls within the range of $r_{ho} = 1.228-1.417\,(\Omega \cdot \mathrm{cm})$. The uniformity of distribution of the mean r_{ho} value over the SW sample is 5.46%.

Photoluminescence (PL) images of SWs before processing (Fig. 8) were also obtained and analyzed. A Luminescence ImaGing System — Model LIS-R1 was used in these measurements. As is known [18], PL images reveal various defects of a wafer related to its positioning in a block (central blocks with a low dislocation density, blocks with a high dislocation density, blocks with impurities in the lower part, side blocks). These defects, in turn, reduce directly the efficiency of finished PVCs [19,20]. Dislocations have a negative effect on both short-circuit current I_{sc} and open-circuit voltage U_{oc}. The specific influence of dislocations and other defects on the performance of finished PVCs is affected directly by the PVC fabrication process (specifically, by the capacity of this process to remove or passivate defects by gettering and hydrogenation). It was concluded based on the results of examination of the initial material that additional DPL passivation of the rear surface is needed.

Values of electrical parameters of fabricated PVCs

PVC type	Number of PVCs, units	V_{oc}, mV	I_{sc}, A	FF, %	R_{sh}, Ω	Efficiency, %
Al-BSF	400	610.3	8.5	76.80	102.3	15.83
PERC	400	650	9.42	79.30	276.1	19.89

Dark regions of PL images of SWs (Fig. 8) are the sites of accumulation of nonradiative recombination centers, which reduce the lifetime of minority carriers to low levels. When the number of defects increases, open-circuit voltage U_{oc} decreases, and this has a negative effect on the PVC performance.

The electrical parameters of PVC batches fabricated in accordance with the standard Al-BSF process and the updated PERC process with PECVD are listed in the table.

It can be seen that the produced PERC PVCs have an efficiency around 20%, which is, on the average, 4% higher than the efficiency of Al-BSF PVCs. The maximum efficiency in the batch of PERC PVCs was 21.01%. It should also be noted that a high value of the open-circuit voltage (650 mV) attests to the excellent passivation properties of the $AlO_x/SiO_xN_y/SiN_1/SiN_2$ layer. The enhanced passivation of the rear surface reduces the number of recombination photogenerated carriers, thus also contributing to an increase in the short-circuit current.

The internal quantum efficiency (IQE) was measured using a Semilab setup and the light-beam-induced current (LBIC) method. IQE is the ratio of the number of charge carriers collected by a photocell to the number of photons of a given energy incident on the PVC surface and absorbed by it. The measurement results are presented in Fig. 9. The obtained data suggest that the absorption of photons proceeds mainly in the visible and red spectral regions.

It also follows from Fig. 9 that PERC PVCs collect more carriers in the 900−1000 nm range than Al-BSF PVCs. This agrees with literature data [16,21], since it was found that the deposition of an Al_2O_3 layer improves the optical reflectivity of the rear PVC surface, thus enhancing the

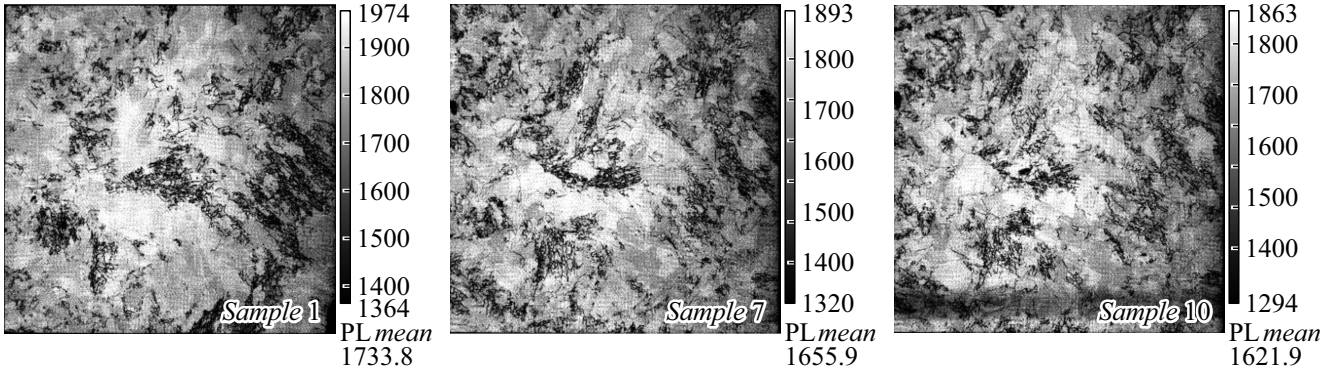

Figure 8. PL images of SWs before processing (samples 1, 7, 10) obtained using a Luminescence ImaGing System — Model LIS-R1.

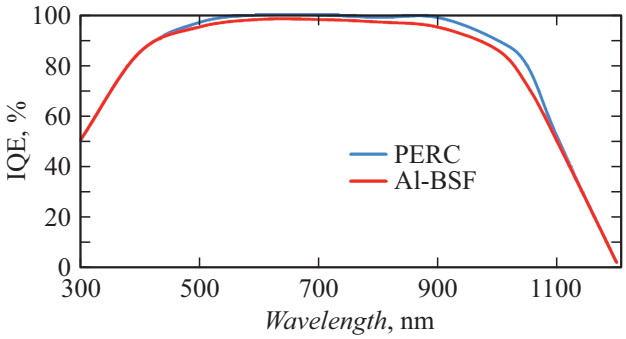

Figure 9. Quantum efficiency of PERC and Al-BSF PVCs.

absorption due to better light interception (especially in the IR range of 700–1000 nm).

Conclusion

Test prototypes of PERC and Al-BSF PVCs were fabricated in the present study. A design of the rear passivation layer deposited by PECVD was proposed. The optimum layer thicknesses were determined: AlO_x — 10 nm, SiO_xN_y — 30 nm, SiN_1 — 50 nm, SiN_2 — 100 nm. The properties of the obtained photoelectric converters were examined. A maximum efficiency of 21.01% was demonstrated for PERC PVCs. Thus, the PVC intensity enhancement in switching to PERC is attributable to the following three key factors: significant suppression of electron recombination; enhancement of the internal reflectivity; and enhancement of light absorption. However, the mechanisms of loss of PVC efficiency require further examination. A modification of the standard production line for PVCs, which are currently fabricated in accordance with the Al-BSF technology at the Kazakhstan Solar Silicon plant, needed to switch to the PERC technology with the PECVD method was proposed.

Conflict of interest

The authors declare that they have no conflict of interest.

References

[1] *United Nations, Department of Economic and Social Affairs, Population Division* (2019). World Population Prospects 2019: Highlights (ST/ESA/SER.A/423)
[2] *ITRPV 2020, International Technology Roadmap for Photovoltaic. Eleventh Edition,* April 2020. https://itrpv.vdma.org/en/
[3] D. Kalygulov, I. Klinovitskaya, T. Turmagambetov, A. Pavlov, S. Plotnikov, B. Mukashev, A. Serikkanov, Z. Agabekov, D. Kantarbaeva. News National Academy Sci. Republic Kazakhstan. Physico-Mathem. Ser., **3** (325), 120 (2019). DOI: 10.32014/2019.2518-1726.18
[4] A.A. Betekbaev, S.V. Plotnikov, D.A. Kalygulov, I.A. Klinovitskaya. Vestn. Evraziiskogo Nats. Univ. Im. L.N. Gumileva, **4** (119), 103 (2017) (in Russian).
[5] T. Dullweber, J. Schmidt. IEEE J. Photovoltaics, **6** (5), 1366 (2016). DOI: 10.1109/JPHOTOV.2016.2571627
[6] A. Blakers. IEEE J. Photovoltaics, **9** (3), 629 (2019). DOI: 10.1109/JPHOTOV.2019.2899460
[7] M.A. Green. Solar Energy Mater. Solar Cells, **143**, 190 (2015). DOI: 10.1016/j.solmat.2015.06.055
[8] A. Kumar, M. Bieri, T. Reindl, A.G. Aberle. Energy Proced., **130**, 43 (2017). DOI: 10.1016/j.egypro.2017.09.412
[9] I.A. Klinovitskaya, S.V. Plotnikov, D.A. Kalygulov. Vestn. Vostochno-Kaz. Tekh. Univ. Im. D. Serikbaeva, **4** (78), 67 (2017) (in Russian).
[10] S.L. Née Werner, M. Meßmer, S. Schmidt, E. Lohmüller, A. Piechulla, A. Wolf. In: *2018 IEEE 7th World Conf. Photovolt. Energy Conversion, WCPEC 2018 — A Jt. Conf. 45th IEEE PVSC, 28th PVSEC 34th EU PVSEC* (Waikoloa, HI, USA, IEEE, 2018), p. 1530–1535. DOI: 10.1109/PVSC.2018.8547603
[11] M.Z. Rahman, S.I. Khan, Mater. Renewable Sustainable Energy, **1**, 1 (2012). DOI: 10.1007/s40243-012-0001-y
[12] B. Min, M. Müller, H. Wagner, G. Fischer, R. Brendel, P.P. Altermatt, H. Neuhaus, IEEE J. Photovoltaics, **7** (6), 1541 (2017). DOI: 10.1109/JPHOTOV.2017.2749007
[13] Sh.K. Chunduri, M. Schmela. PERC Solar Cell Technology, 8, (2017).
[14] J. Schmidt, F. Werner, B. Veith, D. Zielke, S. Steingrube, P.P. Altermatt, S. Gatz, T. Dullweber, R. Brendel. Energy Proced., **15**, 30 (2012). DOI: 10.1016/j.egypro.2012.02.004
[15] K. Matsunaga, T. Tanaka, T. Yamamoto, Y. Ikuhara. Phys. Rev. B. Condens. Matter Mater. Phys., **68** (8), 085110, (2003).
[16] T. Zhou, J.U. Fuchs, V.X. Nguyen, J. Rehli, A. Piechulla, S. Denzer, W. Jooss. In: *31st Eur. Photovolt. Sol. Energy Conf. Exhib,* ed. by S. Rinck, N. Taylor, P. Helm (Hamburg, Germany, WIP Wirtschaft and Infrastruktur GmbH & Co. Planungs-KG, 2015), p. 765. DOI: 10.4229/EUPVSEC20152015-2AV.3.23
[17] H. Huang, J. Lv, Y. Bao, R. Xuan, S. Sun, S. Sneck, S. Li, C. Modanese, H. Savin, A. Wang, J. Zhao. Sol. Energy Mater. Sol. Cells, **161**, 14 (2017). DOI:10.1016/j.solmat.2016.11.018
[18] T. Trupke, B. Mitchell, J.W. Weber, W. McMillan, R.A. Bardos, R. Kroeze. Energy Proced., **15**, 135 (2012). DOI: 10.1016/j.egypro.2012.02.016
[19] W. McMillan, T. Trupke, J. Weber, M. Wagner, U. Mareck, Y.C. Chou, J. Wong. In: *Proc. 25th EU PVSEC, Val. Spain* (Valencia, Spain, WIP Renewable Energies, 2010), p. 134. DOI: 10.4229/25thEUPVSEC2010-2CO.3.5
[20] S. Johnston, F. Yan, K. Zaunbrecher, M. Al-Jassim, O. Sidelkheir, A. Blosse, In: *Conf. Rec. IEEE Photovolt. Spec. Conf.* (IEEE, 2011, 002885-002890), DOI: 10.1109/PVSC.2011.6186549
[21] J.-F. Leliévre, B. Kafle, P. Saint-Cast, P. Brunet, R. Magnan, E. Hernandez, S. Pouliquen, F. Massines. Progr. Photovoltaics: Research and Applications, **27** (11), 1007 (2019). DOI: 10.1002/pip.3141